

Observations of exosphere variations during geomagnetic storms

J. Bailey¹ and M. Gruntman¹

Received 11 March 2013; revised 31 March 2013; accepted 2 April 2013.

[1] The dominant neutral constituent in Earth's upper exosphere, atomic hydrogen (H), resonantly scatters solar Lyman-alpha (121.567 nm) radiation, observed as the geocorona. We report here observations of an exospheric response to geomagnetic storms obtained using measurements of the geocorona by Lyman-alpha detectors on the Two Wide-angle Imaging Neutral-atom Spectrometers mission. We introduce a new parameter, N_H , the number of H atoms in the spherical shell from a geocentric distance of 3 to 8 Earth radii, to quantitatively characterize in a simplified way global exospheric conditions. Five geomagnetic storms observed during three months in the second half of 2011 are accompanied by abrupt temporary increases, spikes, of N_H from 6% to 17%, lasting not longer than a day. These increases seem to show some correlation with the minimum *Dst* index reached during the peak of each storm. **Citation:** Bailey, J., and M. Gruntman (2013), Observations of exosphere variations during geomagnetic storms, *Geophys. Res. Lett.*, 40, doi:10.1002/grl.50443.

1. Introduction

[2] The tenuous extension of Earth's neutral atmosphere, the upper exosphere, consists predominately of atomic hydrogen (H) [e.g., Chamberlain, 1963]. Exospheric H atoms resonantly scatter solar Lyman- α (121.567 nm) radiation, creating a phenomenon known as the geocorona. The Two Wide-angle Imaging Neutral-atom Spectrometers (TWINS) mission [McComas *et al.*, 2009] includes Lyman- α Detectors (LADs) [Nass *et al.*, 2006] to observe the geocorona and investigate exospheric H atoms. We use LAD measurements to reconstruct exospheric H density distributions for geocentric distances from 3 R_E to 8 R_E , where R_E is Earth's mean radius. Our recent publication [Bailey and Gruntman, 2011a] detailed the process of obtaining such distributions, shown to be consistent with prior work. The commonly used observation-based models of Rairden *et al.* [1986] and Østgaard *et al.* [2003] describe the exosphere essentially averaged over significant periods of time such that they rely, respectively, on four years of geocoronal measurements by DE 1 and one year by the IMAGE spacecraft. In contrast, LAD/TWINS often allows obtaining global distributions with three-dimensional asymmetries on a daily basis, which opens a way to

experimentally probe the response of the exosphere to varying solar and geomagnetic conditions. In this letter, we report observed variations of the exosphere during five geomagnetic storms that occurred in the 3 month time period from 1 August 2011 to 31 October 2011.

2. TWINS Lyman- α Experiment

[3] We focus here on observations of the geocorona made from the TWINS-1 satellite, which is in a highly elliptical Molniya-type orbit with a period of one half of a sidereal day. Two Lyman- α detectors, LAD-1 and LAD-2, observe the geocorona for several hours per orbit around apogee from an instrument platform that rotates about a nominally nadir-pointed axis in a $\pm 99^\circ$ windshield wiper motion with a rotational rate of approximately 3° per second [McComas *et al.*, 2009]. Thus, it takes about 1 min for the LADs, pointed at $\pm 40^\circ$ with respect to the rotation axis (Figure 1), to sweep a full circle around the Earth. As the spacecraft proceeds along the orbit, the detectors cover the geocorona, allowing reconstruction of the exospheric H density distribution based on several hours of observations [Bailey and Gruntman, 2011a]. The detectors are single pixel photometers with a field of view of 4° full width at half maximum, spectral band ± 5 nm centered at the wavelength 122 nm, and sensitivity of approximately 2 (cts s^{-1})/ R ($1 R=1$ Rayleigh = $10^6/(4\pi)$ phot $cm^{-2} s^{-1} sr^{-1}$) [Nass *et al.*, 2006]. The platform positions at $\pm 90^\circ$ are such that LAD-1 points in nearly the same direction as LAD-2 in the opposite orientation, and vice versa, allowing for relative cross-calibration of the detectors. The observational geometry usually provides excellent coverage of the Northern Hemisphere, where the TWINS orbit apogee is located, but may be limited in the Southern Hemisphere.

[4] The LAD measured photon intensity is the sum of the geocoronal and interplanetary glows [Bailey and Gruntman, 2011a]. The interplanetary glow occurs as interstellar H atoms inflow into the heliosphere and also resonantly scatter solar Lyman- α radiation. Thus, the intensity, F_P (in Rayleighs), observed by the LADs is

$$F_P = \frac{g^*}{10^6} \int_0^{L_{\max}} n(\bar{L}) I(\alpha) dL + F_{IP} \quad (1)$$

where $n(\bar{L})$ is the local H number density along the line of sight \bar{L} ; $I(\alpha)$ is the angular dependence of Lyman- α photon scattering on atomic hydrogen [Brandt and Chamberlain, 1959]; g^* is the local (adjusted to the actual Earth heliocentric distance) photon scattering rate or g -factor; and F_{IP} is the interplanetary glow (in Rayleighs). For this work, we use daily all-sky maps (W. Pryor, personal communication, 2012) of the interplanetary glow [Pryor *et al.*, 2013] derived directly from SWAN measurements on the SOHO mission.

¹Department of Astronautical Engineering, Viterbi School of Engineering, University of Southern California, Los Angeles, California, 90089-1192, USA.

Corresponding author: J. Bailey, Department of Astronautical Engineering, Viterbi School of Engineering, University of Southern California, Los Angeles, CA 90089-1192, USA. (jjbailey@usc.edu)

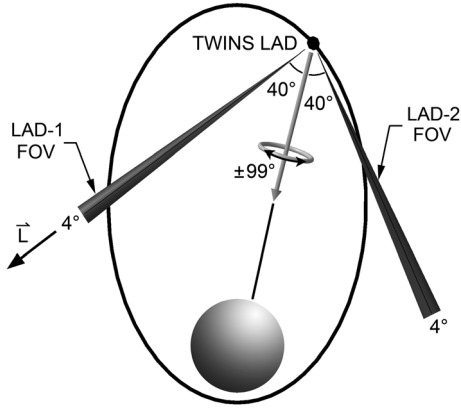


Figure 1. Observational geometry of Lyman- α detectors (LAD-1 and LAD-2) on a TWINS satellite, which is in a highly elliptical Molniya-type orbit with an apogee at a geocentric distance of $7.2 R_E$ (where R_E is Earth's mean radius) over the Northern Hemisphere, inclination of 63.4° , and orbital period of half a sidereal day. Each LAD has a 4° full width at half maximum field of view that is pointed at 40° with respect to the nominally nadir-pointed instrument platform rotation ($\pm 99^\circ$) axis.

3. Model

[5] The experimental and data reduction approach restricts our reconstructed exospheric H density distributions to geocentric distances between $3 R_E$ and $8 R_E$ [Bailey and Gruntman, 2011a]. The lower limit is determined by the requirement of an optically thin geocorona. The interplanetary

glow becomes comparable to or dominates geocoronal intensities beyond the upper limit and introduces uncertainties that make determination of exospheric H densities at larger distances less reliable.

[6] The three-dimensional distribution of H number densities is modeled by a second-order spherical harmonic expansion with 18 free parameters that are best fit to LAD observations using the method of least squares [Bailey and Gruntman, 2011a]. A successful fit predicts measured intensities between 1000 R and 10000 R to within a standard deviation of 125 R. The propagated fitting uncertainty in reconstructed exospheric H number density distributions typically increases from 7% to 9% from $3 R_E$ to $6 R_E$ and then rapidly increases up to 25% at $8 R_E$.

[7] A global fitting is only sensitive to observed regions of the geocorona. The LAD/TWINS experiment requires measurements during a large part of an orbit for adequate coverage around the Earth. Consequently, the experimental data do not allow reconstruction of the global exosphere for time intervals shorter than the several hours of observations that are available along each orbit (orbital period ~ 12 h).

4. Observations

[8] The upper exosphere is a complex three-dimensional distribution of mostly H atoms that usually requires a large number of parameters for its description [Hodges, 1994; Nass et al., 2006; Zoenchen et al., 2010, 2011; Bailey and Gruntman, 2011a]. To gain insight and determine possible dominant drivers of the dynamic exosphere, one could benefit from quantitatively characterizing conditions in a simplified

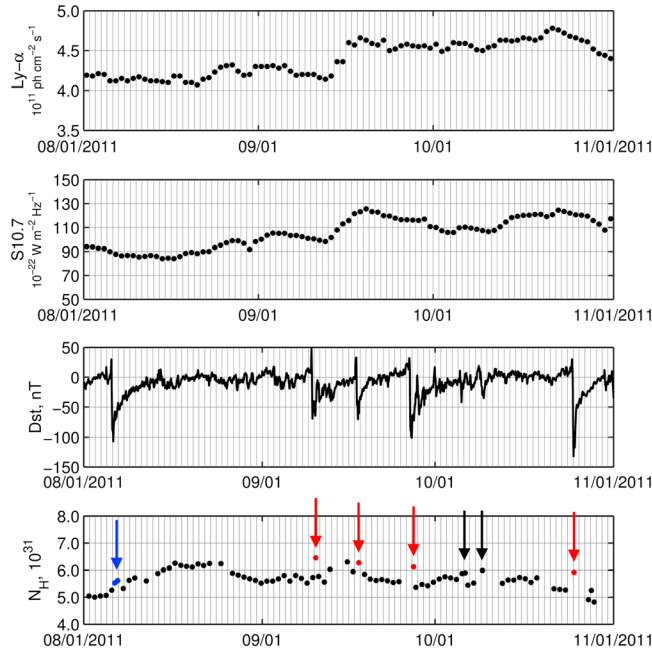


Figure 2. Solar output and exosphere variations during geomagnetic events: (top) daily average composite solar Lyman- α flux at 1 AU [Woods et al., 2000] (data from <http://lasp.colorado.edu/lisird/lya/>, Laboratory for Atmospheric and Space Physics); (second from top) daily average S10.7 index from the Solar Irradiance Platform v2.37 (data from <http://www.spacewx.com/solar2000.html>, Space Environment Technologies); (third from top) hourly disturbance storm time, Dst , index (data from <http://wdc.kugi.kyoto-u.ac.jp/>, Kyoto University); and (bottom) number of H atoms, N_H , in the spherical shell from a geocentric distance of $3 R_E$ to $8 R_E$. The blue and red arrows point to abrupt changes in N_H at the times of five observed geomagnetic storms with $Dst < -60$ nT. The spike on 6 August 2011 (blue arrow) lasts for two orbital coverage periods (total one day). Two black arrows point to N_H increases during intervals of geomagnetic activity with -60 nT $< Dst < -30$ nT.

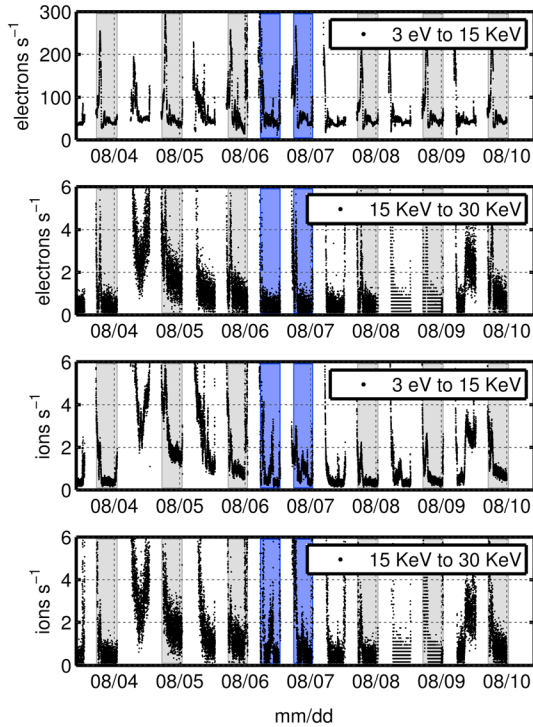


Figure 3. Measurements of two energy bands from 3 eV to 15 keV and 15 keV to 30 keV for electrons (upper two panels) and ions (lower two panels) by the surface charging monitor (SCM). The blue and gray shaded areas are the time intervals (orbits) for which N_H values were obtained by LAD observations. The blue areas correspond to the observed spike in N_H during the storm on 6 August 2011.

way. Here we introduce a new parameter, N_H , the number of H atoms in the spherical shell from a geocentric distance of $3 R_E$ to $8 R_E$, which is obtained from LAD experimental data. Typical H number densities vary from around $400\text{--}1000\text{ cm}^{-3}$ to $10\text{--}100\text{ cm}^{-3}$ at $3 R_E$ and $8 R_E$, respectively. The observed total number of H atoms, N_H , in the selected spherical shell is typically $(4\text{--}7) \times 10^{31}$. The propagated fitting uncertainty, estimated as described in *Bailey and Gruntman* [2011a], is expected to be smaller for the integral quantity of N_H than for three-dimensional H density distributions and it does not exceed 3% for obtained values.

[9] The balance of injection of H atoms to the exosphere and their loss determines the total number of atoms in the shell. Changes in the solar EUV and Lyman- α fluxes as well as geomagnetic activity may cause variation of the injection and loss rates, which would in turn cause changes in N_H . Therefore, this new parameter, N_H , may serve as a measure of global exospheric conditions and provide some insight into its possible correlations with changes in the solar output and geomagnetic activity.

[10] We consider here LAD observations during the 3 month time period from 1 August 2011 to 31 October 2011 when geomagnetic activity finally began to increase after an unusually quiet solar minimum. Five geomagnetic storms occurred during this interval: on 6 August 2011 ($Dst = -107$ nT), 9 September 2011 (-69 nT), 17 September 2011 (-70 nT), 26 September 2011 (-101 nT), and 25 October 2011 (-132 nT) (Figure 2). The bottom panel of Figure 2 shows the temporal variation of N_H obtained by us from

LAD data where one can clearly see abrupt responses, spikes, of exospheric H densities with characteristic times not longer than a day associated with the geomagnetic storms. Figure 2 also shows daily averages of the solar Lyman- α and S10.7 index important to properties of the exosphere. The trajectories of H atoms beyond a few Earth radii are highly susceptible to an effective pressure caused by solar Lyman- α radiation which modifies the three-dimensional distribution and also causes losses. The S10.7 index is the EUV flux between 26–34 nm, contributing to the thermospheric heating and expansion [*Tobiska et al.*, 2008] that affects injection of H atoms into the exosphere as well as their loss due to photoionization.

[11] One can see that N_H exhibits abrupt increases and decreases, spikes, superimposed over more gradual smooth variations that could be caused by seasonal changes of the exosphere [*Bailey and Gruntman*, 2011b] and cumulative responses to changes in the solar X-ray, EUV, and Lyman- α output. In addition, possible systematic effects due to the imperfect observational coverage, which are not yet completely understood but could also result in gradual smooth variations, are not excluded.

[12] The uncertainty introduced by the optically thin assumption could be evaluated [*Bailey and Gruntman*, 2011a] based on detailed simulations of the geocorona by *Bishop* [1999]. The transition from the optically thick to optically thin regime in the geocorona is gradual with increasing geocentric distance. We tested the adopted $3 R_E$ boundary assumption for the lower limit by refitting the results to a $4 R_E$ boundary and obtained nearly the same N_H spikes.

[13] The possibility that the observed N_H spikes are detector artifacts caused by the local energetic particle environment seems to be unlikely. Two of the Geostationary Operational Environmental Satellites, GOES-13 and -15, reported (<http://www.swpc.noaa.gov/today.html>) intensities of protons (≥ 10 MeV) and electrons (≥ 2 MeV) at geostationary orbit during the considered geomagnetic storms that did not exceed specified alert levels of $10\text{ protons cm}^{-2}\text{ s}^{-1}\text{ sr}^{-1}$ and $1000\text{ electrons cm}^{-2}\text{ s}^{-1}\text{ sr}^{-1}$, respectively. Similarly, in situ particle fluxes measured by environmental monitors on the TWINS-1 spacecraft were also minimal such that artifacts in LAD measurements, particularly due to high energy (\sim MeV)

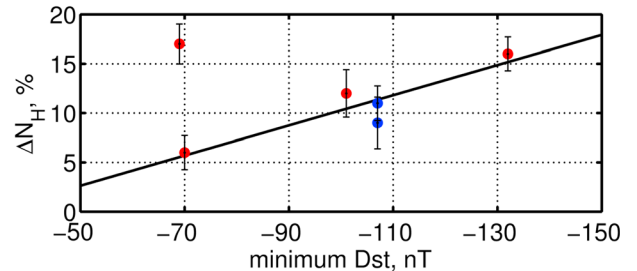


Figure 4. Minimum Dst index for five observed geomagnetic storms versus the corresponding relative ΔN_H increases with error bars for the estimated fitting uncertainty. The straight line is a linear fit of the minimum Dst index and ΔN_H if one excludes the data point for 9 September 2011 at 17% and -69 nT. The longer duration of an effective main phase may have contributed to the higher observed ΔN_H increase for this event. The color coding of events is similar to that in Figure 2.

Table 1. Minimum Dst Index and the Corresponding Relative ΔN_H Increases for Five Geomagnetic Storms ($Dst < -60$ nT) Observed in the 3 Month Time Period From 1 August 2011 to 31 October 2011; Estimated Fitting Uncertainty is Less Than 3% for All Obtained N_H Values

Date	Dst , nT	ΔN_H , %
6 August 2011	-107	9, 11
9 September 2011	-69	17
17 September 2011	-70	6
26 September 2011	-101	12
25 October 2011	-132	16

electrons that could penetrate the sensor and trigger the channel electron multipliers, would not be expected.

[14] The TWINS-1 spacecraft carries two types of environmental monitors [McComas *et al.*, 2009]. A three-channel dosimeter (DOS) measures electrons (protons) with energies ≥ 1.5 (16) MeV and ≥ 3 (25) MeV (T. Guild, personal communication, 2012). An electrostatic plasma analyzer that serves as a surface charging monitor (SCM) measures charged particles from 3 eV to 30 keV. We analyzed the in situ particle fluxes observed by DOS and SCM (Figure 3) for the few days before (quiet-time conditions; gray shaded in Figure 3), during (blue shaded), and after (gray shaded) all five storms to specifically establish any possible correlation with LAD measurements.

[15] The reported fluxes of energetic particles measured by the DOS monitor were zero, as expected, when the LADs were taking measurements above an orbital radius of approximately $4.5 R_E$. Figure 3 presents, as an example, fluxes measured by SCM in two energy bands from 3 eV to 15 keV and 15 keV to 30 keV for electrons (Figure 3, upper two panels) and ions (Figure 3, lower two panels) during the storm on 6 August 2011. If electrons and/or ions were to somehow “leak” into the LADs and trigger the photon-counting detectors, then one would anticipate correspondingly higher fluxes of particles during the observed N_H spikes. One can see, however, that the particle fluxes are typically higher during orbits either preceding or following the orbits of the observed N_H enhancement. Therefore, it seems unlikely that the observed N_H enhancement was caused by an increase in local fluxes of electrons and ions. Other storms exhibit similar particle fluxes as in the example above.

[16] To conclude, LAD measurements did not show correlation with the in situ particle fluxes observed by DOS and SCM for the few days before (quiet-time conditions), during, and after all five storms. Consequently, the possibility that the observed N_H enhancements are detector artifacts caused by the local energetic particle environment is not supported by the TWINS environmental monitors. The described procedure of assessing environmental fluxes during geomagnetic events could be applied for ruling out possible artifacts in future LAD measurements.

[17] Table 1 lists for each geomagnetic storm the minimum Dst index and the observed relative ΔN_H increase. All five observed storms with $Dst < -60$ nT are accompanied by spikes in N_H , indicated by blue and red arrows in Figure 2 (bottom), from 6% to 17% (Table 1). The spike on 6 August 2011 (blue arrow) reveals a ΔN_H increase lasting for two orbits, or one day. The red arrows point to spikes that last only half a day (e.g., 9 September 2011) or for which an N_H value from the orbit prior to the event (e.g., on 26 September 2011) as well as the orbits prior and immediately after the event (e.g., on 25 October 2011) are not available. The N_H values immediately before and

after the spike on 9 September 2011 are equal to each other within 1%. Clearly, the introduced simple parameter, N_H , shows enhancements associated with all standalone Dst events that decrease below -60 nT.

[18] On the other hand, two observed N_H increases on 15 September 2011 and 28 October 2011 appear uncorrelated with geomagnetic disturbances. In addition, two black arrows point to N_H enhancements during intervals of geomagnetic activity with significantly smaller Dst decreases (above -50 nT). There is also uncertainty about a spike on 9 October 2011 (right black arrow) because N_H values for the orbits immediately before and after the event are not available.

[19] Figure 4 presents the minimum Dst index for each observed storm ($Dst < -60$ nT) versus the corresponding relative ΔN_H increases. A nearly linear dependence emerges between the minimum Dst index and ΔN_H if we exclude 9 September 2011. While it cannot be ruled out that this apparent outlier is due to sparse coverage of the storm time, it seems that it is more likely caused by a peculiar Dst dependence, as discussed below, of that storm. Note that uncertainty

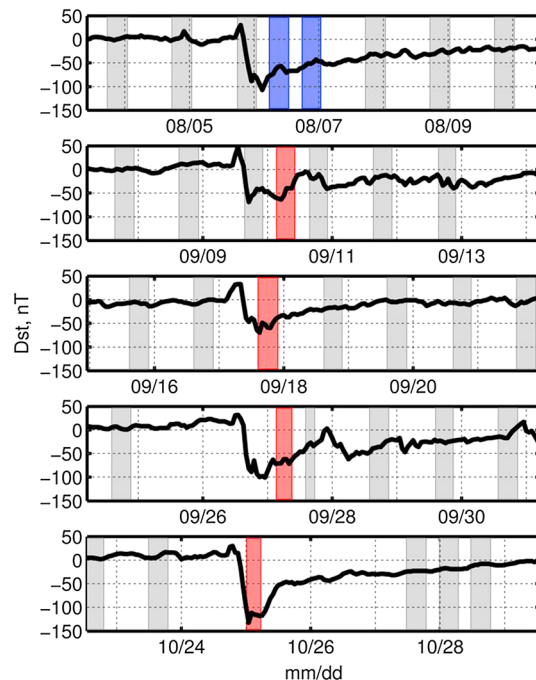


Figure 5. Time intervals (orbits) of obtained sparse N_H data points and disturbance storm time, Dst , index (data from <http://wdc.kugi.kyoto-u.ac.jp/>, Kyoto University) during five observed geomagnetic storms. The blue, red, and gray shaded areas are the time intervals (orbits) for which N_H values were obtained by LAD observations. The red and blue areas correspond to the observed spikes in N_H . The color coding of events is similar to that in Figure 2.

of the daily solar Lyman- α averages (Figure 2, top) is significantly smaller than the estimated errors of the ΔN_H increases (Figure 4). In addition, no noticeable solar flares occurred during the times of the observed N_H enhancements.

[20] The obtained N_H data points are sparse and do not cover storm phases uniformly in time. Figure 5 shows the hourly Dst index during each of the observed storms and orbital coverage periods (shaded areas) where it was possible to obtain N_H values. Only for two storms, 6 August 2011 and 9 September 2011, were we able to obtain three consecutive values of N_H .

[21] The storm on 9 September 2011 seems to differ from the other four storms. One can see that all other storms follow relatively similar Dst profiles for the sudden commencement, initial, main, and recovery phases. The storm on 9 September 2011 reaches its minimum Dst index of -69 nT at 1700 UTC and then 12 h later drops again to -64 nT at 0500 UTC on the following day before finally beginning to recover. The longer duration of an effective main phase may have contributed to the higher observed ΔN_H increase for this event. More storm observations are needed to better establish the relationship, as well as gain some insight into the possible causal link, between geomagnetic activity and exospheric H density enhancements.

5. Conclusions

[22] TWINS-1 LAD measurements from 1 August 2011 to 31 October 2011 revealed temporal variations of the exosphere during geomagnetic storms. We introduce a new parameter, N_H , to quantitatively characterize in a simplified way exospheric conditions in the spherical shell from a geocentric distance of $3 R_E$ to $8 R_E$. Abrupt temporary increases in the total number of H atoms in this shell, from 6% to 17%, have been recorded for five observed storms from 6 August 2011 to 25 October 2011. The increases seem to show some correlation with the minimum Dst index reached during the peak of each storm.

[23] As initially described by Chamberlain [1963], the exosphere comprises three main particle populations: ballistic, escaping, and satellite. The orbital periods of satellite atoms increase from 0.3 to 1.3 days for orbit semimajor axes increasing from $3 R_E$ to $8 R_E$. The lifetime of H atoms in satellite orbits could thus be up to several days while the observed N_H enhancements last not longer than a day. This difference seems to limit if not eliminate the possible contribution by satellite H atoms to the observed N_H increases. In contrast, a ballistic H atom leaving the exobase (~ 500 km altitude) or produced in the plasmasphere and reaching an apogee of $8 R_E$ and returning back would have a roundtrip time-of-flight 13–18 h, consistent with the observed N_H increases lasting half a day or perhaps one day. Future observations of more geomagnetic storms with better coverage in time and examination of altitude dependences of H density enhancements may help to better understand the exospheric response as well as the possible coupling effects via charge exchange that exist between the exosphere and plasmasphere.

[24] Our proposed characterization of the exosphere by the total number of H atoms, N_H , in a selected spherical shell looks promising for investigation of possible effects and specific mechanisms of interaction with the solar output, magnetosphere, and plasmasphere. We note that the observed denser exosphere in the spherical shell from $3 R_E$

to $8 R_E$ during storms would increase ring current loss rates due to charge exchange. Interpretation of magnetospheric images in energetic neutral atom fluxes essentially relies on a line-of-sight integration that directly depends on the H number density distribution [Williams *et al.*, 1992; Gruntman, 1997; McComas *et al.*, 2009]. Consequently, temporal variations of the exosphere during storms are of particular interest for energetic neutral atom imaging of the magnetosphere.

[25] **Acknowledgments.** The authors gratefully thank the TWINS team (PI Dave McComas); Hans Fahr, Uwe Nass, and Jochen Zoennchen of the LAD team; and Tim Guild, Margaret Chen, and Michael Redding who provided energetic particle environmental data and helped with their analysis. We acknowledge support by W. Kent Tobiska with solar irradiance data and Wayne Pryor for providing the interplanetary glow maps. We also thank the reviewers for very helpful comments and suggestions. This work is supported in part by the NASA TWINS mission. J. B. acknowledges support by a Northrop Grumman fellowship.

[26] The Editor thanks Nikolai Østgaard and an anonymous reviewer for their assistance in evaluating this paper.

References

- Bailey, J., and M. Gruntman (2011a), Experimental study of exospheric hydrogen atom distributions by Lyman-alpha detectors on the TWINS mission, *J. Geophys. Res.*, *116*, A09302, doi:10.1029/2011JA016531.
- Bailey, J., and M. Gruntman (2011b), Seasonal variations of the exosphere as observed by Lyman-alpha detectors on the TWINS mission, Abstract SM13D-2102 presented at 2011 Fall Meeting, AGU, San Francisco, Calif., 5-9 Dec.
- Bishop, J. (1999), Transport of resonant atomic hydrogen emissions in the thermosphere and geocorona: Model description and applications, *J. Quant. Spectrosc. Radiat. Transf.*, *61*(4), 473–491, doi:10.1016/S0022-4073(98)00031-4.
- Brandt, J. C., and J. W. Chamberlain (1959), Hydrogen radiation in the night sky, *Astrophys. J.*, *130*, 670–682, doi:10.1086/146756.
- Chamberlain, J. W. (1963), Planetary coronae and atmospheric evaporation, *Planet. Space Sci.*, *11*, 901–960, doi:10.1016/0032-0633(63)90122-3.
- Gruntman, M. (1997), Energetic neutral atom imaging of space plasmas, *Rev. Sci. Instrum.*, *68*, 3617–3656, doi:10.1063/1.1148389.
- Hodges, R. R. (1994), Monte Carlo simulation of the terrestrial hydrogen exosphere, *J. Geophys. Res.*, *99*, 23229–23247, doi:10.1029/94JA02183.
- McComas, D. J., et al. (2009), The Two Wide-angle Imaging Neutral-atom Spectrometers (TWINS) NASA Mission-of-Opportunity, *Space Sci. Rev.*, *142*, 157–231, doi:10.1007/s11214-008-9467-4.
- Nass, H. U., J. H. Zoennchen, G. Lay, and H. J. Fahr (2006), The TWINS-LAD mission: Observations of terrestrial Lyman- α fluxes, *Astrophys. Space Sci. Trans.*, *2*, 27–31, doi:10.5194/astro-2-27-2006.
- Østgaard, N., S. B. Mende, H. U. Frey, G. R. Gladstone, and H. Lauche (2003), Neutral hydrogen density profiles derived from geocoronal imaging, *J. Geophys. Res.*, *108*(A7), 18–1, doi:10.1029/2002JA009749.
- Pryor, W. R., G. M. Holsclaw, W. E. McClintock, M. Snow, R. J. Vervack, Jr., G. R. Gladstone, S. A. Stern, K. D. Retherford, and P. Miles (2013), Lyman-alpha models for LRO LAMP from MESSENGER MASCS and SOHO SWAN data, in *Cross-Calibration of Far UV Spectra of Solar System Objects and the Heliosphere*, ISSI Scientific Report Series 13, pp. 163–175, edited by E. Quémerais, M. A. Snow, and R.-M. Bonnet, Springer, New York, doi:10.1007/978-1-4614-6384-9_5.
- Rairden, R. L., L. A. Frank, and J. D. Craven (1986), Geocoronal imaging with dynamics explorer, *J. Geophys. Res.*, *91*(A12), 13613–13630, doi:10.1029/JA091iA12p13613.
- Tobiska, W. K., S. D. Bouwer, and B. R. Bowman (2008), The development of new solar indices for use in thermospheric density modeling, *J. Atm. Solar-Terr. Phys.*, *70*, 803–819, doi:10.1016/j.jastp.2007.11.001.
- Williams, D. J., E. C. Roelof, and D. G. Mitchell (1992), Global magnetospheric imaging, *Rev. Geophys.*, *30*, 183–208, doi:10.1029/92RG00732.
- Woods, T. N., W. K. Tobiska, G. J. Rottman, and J. R. Worden (2000), Improved solar Lyman α irradiance modeling from 1947 through 1999 based on UARS observations, *J. Geophys. Res.*, *105*(A12), 27195–27215, doi:10.1029/2000JA000051.
- Zoennchen, J. H., U. Nass, G. Lay, and H. J. Fahr (2010), 3-D-geocoronal hydrogen density derived from TWINS Ly- α -data, *Ann. Geophys.*, *28*, 1221–1228, doi:10.5194/angeo-28-1221-2010.
- Zoennchen, J. H., J. J. Bailey, U. Nass, M. Gruntman, H. Fahr, and J. Goldstein (2011), The TWINS exospheric neutral H-density distribution under solar minimum conditions, *Ann. Geophys.*, *29*, 2211–2217, doi:10.5194/angeo-29-2211-2011.